

DOE/BC/15110-3
(OSTI ID: 753863)

USING CHEMICALS TO OPTIMIZE CONFORMANCE CONTROL IN
FRACTURED RESERVOIRS

Semi-Annual Report
October 1, 1999-March 31, 2000

By
Randall S. Seright.

Date Published: April 2000

Work Performed Under Contract No. DE-AC26-98BC15110

New Mexico Petroleum Recovery Research Center
New Mexico Institute of Mining and Technology
Socorro, New Mexico



National Petroleum Technology Office
U.S. DEPARTMENT OF ENERGY
Tulsa, Oklahoma

DISCLAIMER

This report was prepared as an account of work sponsored by an agency of the United States Government. Neither the United States Government nor any agency thereof, nor any of their employees, makes any warranty, expressed or implied, or assumes any legal liability or responsibility for the accuracy, completeness, or usefulness of any information, apparatus, product, or process disclosed, or represents that its use would not infringe privately owned rights. Reference herein to any specific commercial product, process, or service by trade name, trademark, manufacturer, or otherwise does not necessarily constitute or imply its endorsement, recommendation, or favoring by the United States Government or any agency thereof. The views and opinions of authors expressed herein do not necessarily state or reflect those of the United States Government.

This report has been reproduced directly from the best available copy.

Using Chemicals to Optimize Conformance Control in Fractured Reservoirs

By
Randall S. Seright

April 2000

Work Performed Under Contract No DE-AC26-98BC15110

Prepared for
U.S. Department of Energy
Assistant Secretary for Fossil Energy

Tom Reid, Project Manager
National Petroleum Technology Office
P.O. Box 3628
Tulsa, OK 74101

Prepared by
New Mexico Petroleum Recovery Research Center
New Mexico Institute of Mining and Technology
801 Leroy Place
Socorro, NM 87801-4796

TABLE OF CONTENTS

Abstract	v
Project Objectives	1
Gel Propagation Through Fractures	1
New Model	1
Effect of Fracture Width	2
Physical Basis for Eq. 1	3
Model Predictions in Long Fractures	4
Disproportionate Permeability Reduction	6
Imaging Experiments Using Synchrotron X-Ray Microtomography	6
Effect of Temperature on the Disproportionate Permeability Reduction	14
Summary	14
References	15

ABSTRACT

This technical progress report describes work performed from October 1, 1999, through March 31, 2000, for the project, "Using Chemicals to Optimize Conformance in Fractured Reservoirs." During extrusion of gels through fractures, a simple relation ($u_l = 0.05 t^{-0.55}$, where u_l is water leakoff rate in $\text{ft}^3/\text{ft}^2/\text{d}$ or ft/d and t is time in days) described gel dehydration over a wide range of conditions. A model based on this equation was applied to estimate how far gels penetrate into two-wing fractures, as a function of injection rate and fracture width. The results demonstrate that to maximize gel penetration along a given fracture, gel should be injected at the highest practical injection rate.

Imaging experiments are in progress using high-resolution computed microtomography (CMT) at Brookhaven National Laboratory to understand why gels reduce permeability to water more than that to oil. The method provides outstanding resolution of rock, water, and oil on a micrometer scale. In water-wet Berea sandstone, the water film around trapped residual oil drops was clearly visible. In our first set of experiments, CMT results indicated that gels increased the residual oil saturation in larger pores during water injection, thus decreasing permeability to water much more than that to oil.

We also began a study of the effects of temperature on the ability of gels to reduce permeability to water more than that to oil. With a Cr(III)-acetate-HPAM gel in water-wet Berea sandstone, the disproportionate permeability reduction was substantial at temperatures of 41 °C, 60°C, and 80°C. Water permeability was reduced 34 to 240 times more than that to oil. Additional work is required to understand details of the effects of temperature on the disproportionate permeability reduction.

PROJECT OBJECTIVES

This research project has three objectives. The first objective is to develop a capability to predict and optimize the ability of gels to reduce permeability to water more than that to oil or gas. The second objective is to develop procedures for optimizing blocking-agent placement in wells where hydraulic fractures cause channeling. The third objective is to develop procedures to optimize blocking-agent placement in naturally fractured reservoirs. This research project consists of three tasks, each of which addresses one of the above objectives. Our work is directed at both injection wells and production wells and at vertical, horizontal, and highly deviated wells.

GEL PROPAGATION THROUGH FRACTURES

New Model. Recently¹, we introduced a new model for gel propagation and dehydration during extrusion through fractures. This model was based on Eq. 1, which described the rate of water leakoff (u_l , in ft³/ft²/d or ft/d) from the gel through a fracture face during gel extrusion.

$$u_l = 0.05 t^{0.55} \dots\dots\dots (1)$$

In this equation, t is time in days. Eq. 1 was based on a fit of leakoff data from seven experiments (Fig. 1), in which 24-hr-old Cr(III)-acetate-HPAM gels were extruded through seven separate fractured cores (650-mD Berea sandstone). Specifically, our experiments used an aqueous gel that contained 0.5% Ciba Alcoflood 935 HPAM (molecular weight $\approx 5 \times 10^6$ daltons; degree of hydrolysis 5% to 10%), 0.0417% Cr(III) acetate, 1% NaCl, and 0.1% CaCl₂ at pH=6. All experiments were performed at 41°C (105°F). The gelant formulations were aged at 41°C for 24 hours (5 times the gelation time) before injection into a fractured core. All fractures had nominal widths of 0.04 in. The fracture dimensions in these experiments were 48x1.5x0.04 in., 12x12x0.04 in., or 6x1.5x0.04 in. Gel injection velocities (fluxes), based on the cross-section of the fracture, ranged from 129 to 33,100 ft/d. Eq. 1 provided an excellent description of the water leakoff data from these experiments (Fig. 1). Details can be found in Ref. 1.

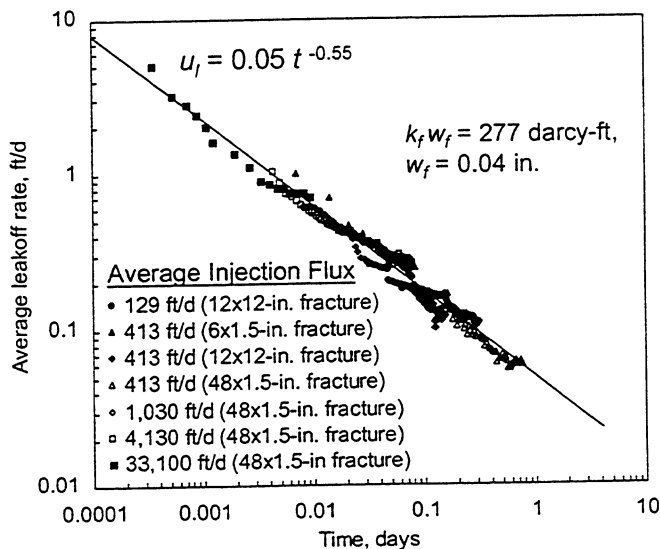


Fig. 1—Average leakoff rates in 0.04-in.-wide fractures.

Effect of Fracture Width. The above model worked well in describing the rate of gel propagation and the rate of water leakoff in fractures with widths of 0.04 in. Will the model require substantial modification if the fracture width is some other value? Fig. 2 shows leakoff results from four experiments where our standard 24-hr-old Cr(III)-acetate-HPAM gel was extruded through 0.08-in.-wide fractures (fracture dimensions: 48x1.5x0.08 in.) at fluxes ranging from 207 to 16,500 ft/d. These experimental results generally followed the trend described by Eq. 1 (the solid line in Fig. 2); however, the fit was less impressive than that shown in Fig. 1.

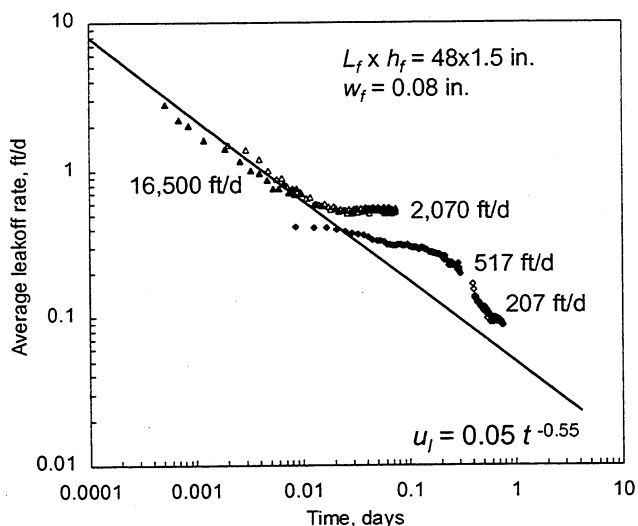


Fig. 2—Average leakoff rates in 0.08-in.-wide fractures.

We also performed high-rate (16,000 cm³/hr) extrusion experiments in fractures with widths of 0.02, 0.04, 0.08, and 0.16-in. (The length and height of the fractures were 48 in. and 1.5-in., respectively, and 3.7 liters of our standard 24-hr-old Cr(III)-acetate-HPAM gel were injected.) Fig. 3 shows that Eq. 1 described the results reasonably well.

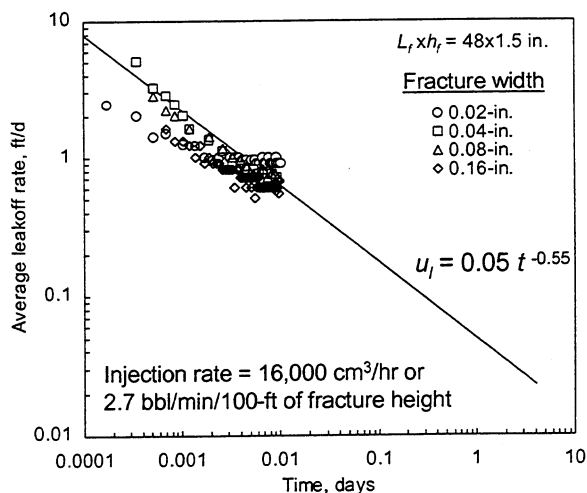


Fig. 3—Average leakoff rates for different fracture widths.

Physical Basis for Eq. 1. What is the physical basis for Eq. 1? Because leakoff varies approximately with the square root of time, one might guess that the relation is analogous to the formation of a filter cake during hydraulic fracturing.² However, important differences exist. For normal (incompressible) filter cake formation, a cake forms with permeability, k , and uniform thickness, L . For a given pressure difference, Δp , and solvent viscosity, μ , the solvent flux (leakoff rate), u , through the filter cake is given by the Darcy equation.

$$u = k\Delta p/(\mu L) \dots\dots\dots(2)$$

The filter cake thickness increases with solvent throughput according to Eq. 3.

$$L = C \int u dt \dots\dots\dots(3)$$

Combining Eqs. 2 and 3, the leakoff rate is easily shown to vary with the square root of time.²

However, in our problem, where water leakoff occurs during gel extrusion through a fracture, a filter cake of uniform thickness does not form. In particular, we have not observed a gel concentration variation (i.e., a filter cake) in the width direction of the fracture. In contrast, we have noted gel concentration variations along the length and height directions. These latter variations were caused by mobile gel (with a composition of the originally injected gel) that wormholed through immobile, concentrated (dehydrated) gel.³

Our current picture of the gel propagation and dehydration process is as follows: When the gel front first contacts a new element of fracture area, the gel in this vicinity basically has the same composition as that for the originally injected gel.³ The permeability of this gel to water is relatively high—around 1 mD.¹ Consistent with these observations, the rate of water leakoff (i.e., leakoff flux) from the gel (and fracture) is greatest just upstream of the gel front.³ As the water leaks off from the gel, the gel concentrates and becomes immobile in the vicinity where the dehydration occurred. The next element of fresh (mobile) gel must find its way around or through (i.e., wormhole through) the concentrated gel in order to advance the gel front. With time at a given position along the fracture, our experiments reveal that the average gel concentration increases and the fracture area contacted by wormholes (i.e., mobile gel) decreases.^{3,4}

At any given distance along the length of a fracture, a fraction of the fracture area will be contacted by immobile, concentrated gel, while the remaining area will be contacted by mobile gel (where the wormholes exist). Thus, two separate sources contribute to leakoff—(1) concentrated, immobile gel that was formed from the dehydration process and (2) mobile gel. The immobile gel continually concentrates during the extrusion process.⁴ We believe that this contribution is minor for the vast majority of the extrusion process because gel permeability to water varies inversely with the third power of gel concentration.¹ As the immobile gel in the fracture becomes more concentrated, its ability to squeeze out additional water rapidly decreases. Furthermore, experimental studies (using leakoff of dyed water), demonstrated that the dominant source of leakoff was from second source—from the mobile gel in the wormholes.¹ When an

element of mobile gel dehydrates, presumably a thin filter cake of concentrated gel forms on the fracture wall. However, because we have never physically observed this thin layer, we assume that it must be quickly torn and swept to the side (by water trying to reach the fracture face) to merge with the concentrated immobile gel.

For the gel propagation and dehydration model that we propose, Eq. 1 implies that the fracture area contacted by wormholes must vary with $t^{0.55}$. Fig. 4 plots our specific predictions of fracture area contacted by fresh gel, a_f , and concentrated gel, a_c , versus gel-contact time. A physical explanation for the variation of total wormhole area, a_p , with time is currently being investigated.

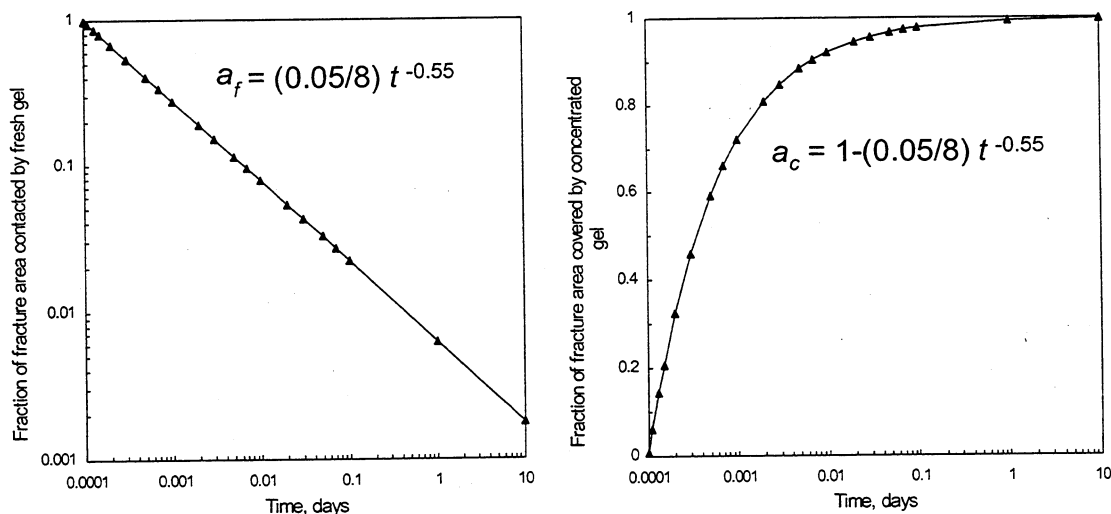


Fig. 4—Predictions of fraction of fracture area contacted by fresh versus concentrated gel.

Model Predictions in Long Fractures. A key motivation for this work is a need to quantify how gels propagate through fractures in field applications. Of course, these fractures are much longer and higher than those examined experimentally in our research. To accurately predict behavior in field applications, a satisfactory model is required for gel propagation and dehydration during extrusion. Further testing is needed to establish whether we have the correct model. Nevertheless, the new model was applied to make predictions for field applications. Fig. 5 presents these predictions for three injection rates (0.1 to 10 barrels per minute, BPM) in 0.04-in.-wide, two-wing fractures using our standard Cr(III)-acetate-HPAM gel. At a given rate, Fig. 5 shows the gel volume that must be injected to achieve a given distance of penetration along the fracture. This volume increased with distance of penetration raised approximately to the 1.5 power. For a given distance of penetration, the required gel volume decreased substantially with increased injection rate. For example, to penetrate 200 ft, the required gel volume was 5 times less at 10 BPM than at 1 BPM. Therefore, to maximize gel penetration, the highest practical injection rate should be used.

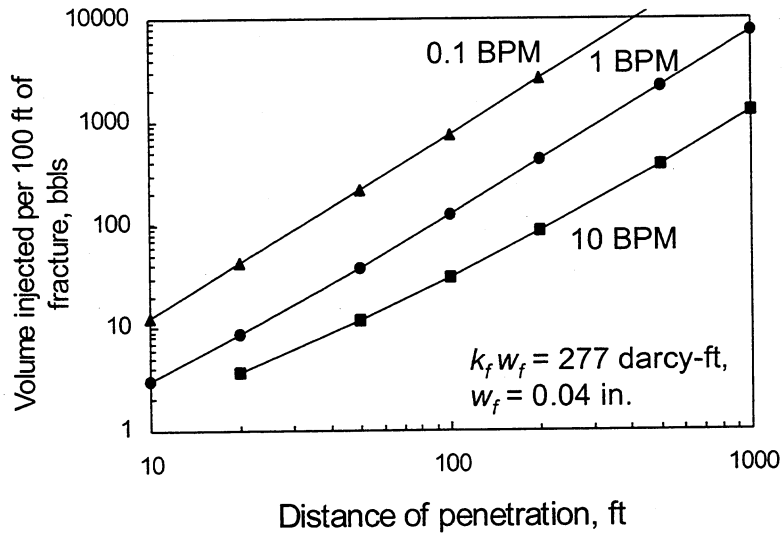


Fig. 5—Model predictions in long two-wing fractures at different rates.

At this point, it may be overly optimistic to expect Eq. 1 to be generally valid for all fracture widths. Nevertheless, out of curiosity, we applied the model assuming that it was valid for fracture widths ranging from 0.01 to 1 in. Fig. 6 plots the predicted distances of gel penetration versus the volume of gel injected for three fracture widths during gel injection at 1 barrel per minute. Interestingly, the curves came together at high distances of penetration and low fracture widths. This result occurred because the rate of gel propagation was governed increasingly by the rate of gel dehydration (i.e., water leakoff given by Eq. 1) as fracture width decreased or as the desired distance of gel penetration increased. In contrast, for a fixed injection rate, gel propagation was governed simply by the fracture width (or volume) for large fracture widths or small distances of gel penetration.

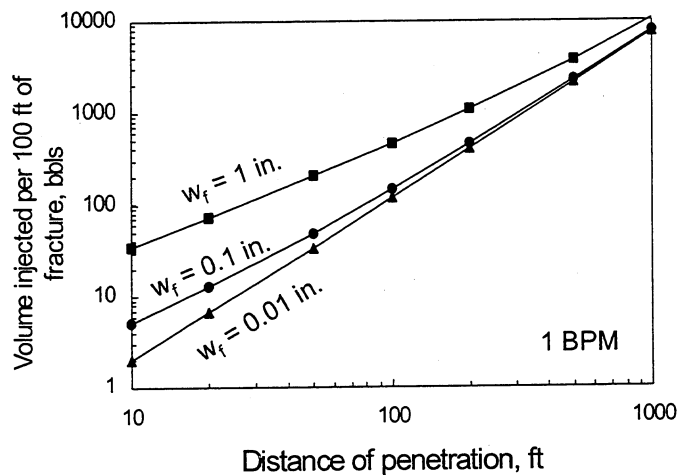


Fig. 6—Model predictions in long two-wing fractures with different widths.

DISPROPORTIONATE PERMEABILITY REDUCTION

Imaging Experiments Using Synchrotron X-Ray Microtomography. We performed imaging experiments using high-resolution computed microtomography (CMT) to compare the oil and water pathways as well as the fluid distribution before and after gel treatment. The imaging experiments were performed in collaboration with ExxonMobile Research & Engineering company at the National Synchrotron Light Source (NSLS) at Brookhaven National Laboratory. The objective was to study the disproportionate permeability reduction on a microscopic scale.

Previously, we used NMR imaging to observe disproportionate permeability reduction on a microscopic scale.⁵ Results from these experiments revealed that the imaging technique had many limitations that prevented us from obtaining reliable pore-level images. Most importantly, the spatial resolution was on the order of hundreds of micrometers, which was too low to clearly distinguish fluid pathways on the pore level. Recent advancements in computed microtomography using synchrotron X-ray sources provides the ability to obtain three-dimensional pore-level images of rock samples with a spatial resolution on the order of micrometers.⁶ This technology has been available at the National Synchrotron Light Source for many years. Recent improvements in data acquisition, transmission, and reconstruction have reduced the time required to produce 3-D pore-level images to a few hours, which is a fraction of the time required in previous scanning methods.

Fig. 7 shows a schematic of the CMT apparatus. To produce an image slice, X-rays transmitted through the sample are recorded on a linear array of detectors. The sample is rotated by a discrete angular interval determined by the linear resolution desired. The procedure is repeated for each angular view until the sample has been rotated by 180° in the X-ray beam. The data collected during the process are then used to reconstruct the horizontal slice. The CCD camera is capable of reconstructing 1,000 horizontal slices simultaneously. Instead of detecting X-ray transmission directly, which limits the spatial resolution to the detector size, a thin high-resolution scintillator placed behind the sample converts each X-ray attenuation map to a visible image, which is then magnified and re-imaged with conventional optics onto the cooled CCD area array.

The core (high-permeability Berea sandstone) was 6.5 mm in diameter and 30 mm in length with an intermediate pressure tap 6 mm from the inlet face (Fig. 8). Due to the computer memory and time constraints, we focused our scan in a segment of the core that was 6.5 mm in diameter and 3.25 mm in length. To avoid end effects, the scanned segment was located about half way between the inlet and outlet faces (Fig. 8). The gel was our standard Cr(III)-acetate-HPAM. Hexadecane was the oil phase. To increase the image contrast between the brine and the oil phases, hexadecane was doped with 10% w/w iodo-hexadecane. All experiments were performed at room temperature. To digitally compare the images before and after gel placement, oil, water, and gelant flooding were performed without ever removing the core from the sample stand. In total, we performed six 3-D scans with an image resolution of 10 μm at different stages of the oil-water experiment. During the imaging experiments, we first scanned the core when it was saturated only with brine. Next, the core was scanned at residual water saturation and residual oil saturation before gelant injection. After gel placement, the core shut in for twelve hours (at ~60°C) and then scanned.

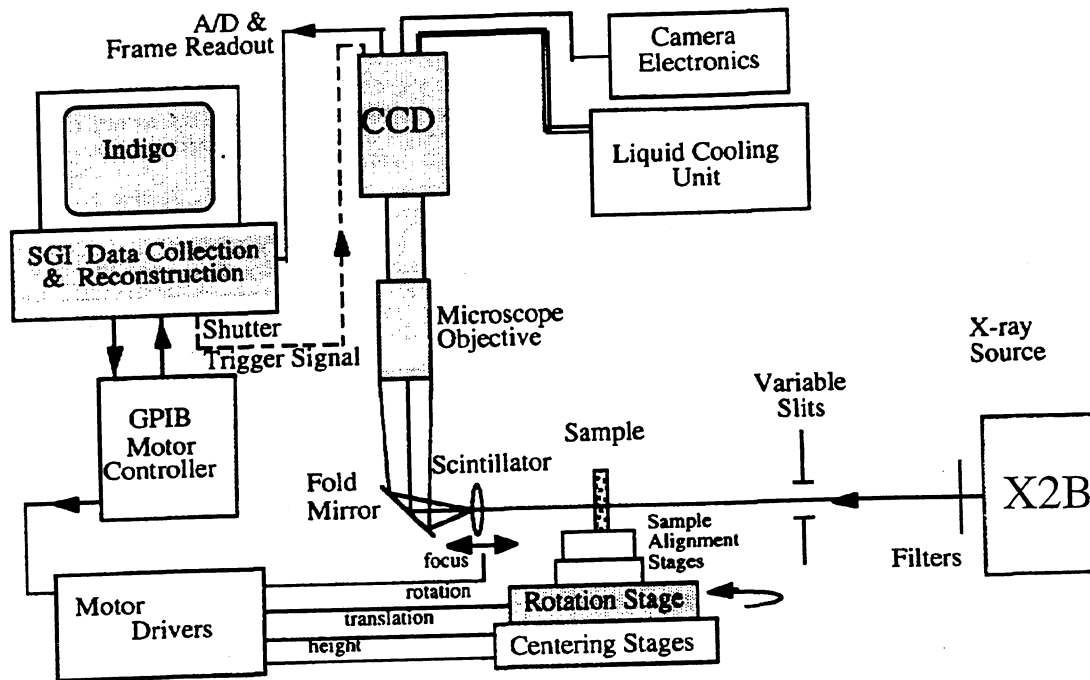


Fig. 7—Schematic of X-ray Synchrotron Microtomography apparatus.

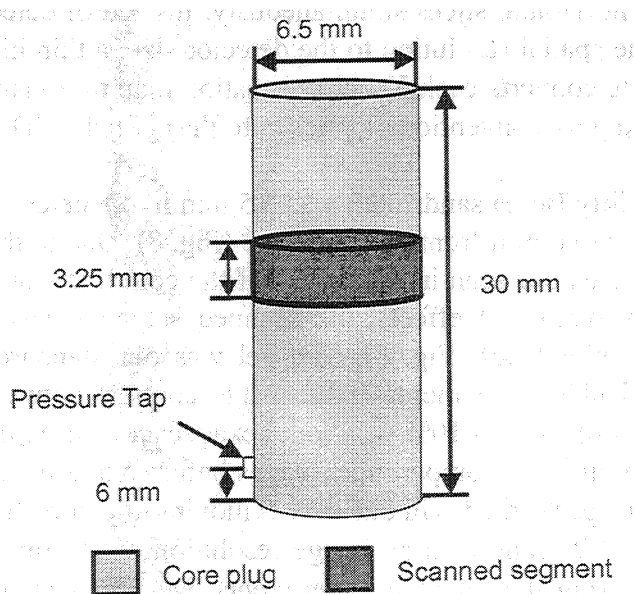


Fig. 8—1,000-md Berea core plug used in X-ray Synchrotron Microtomography

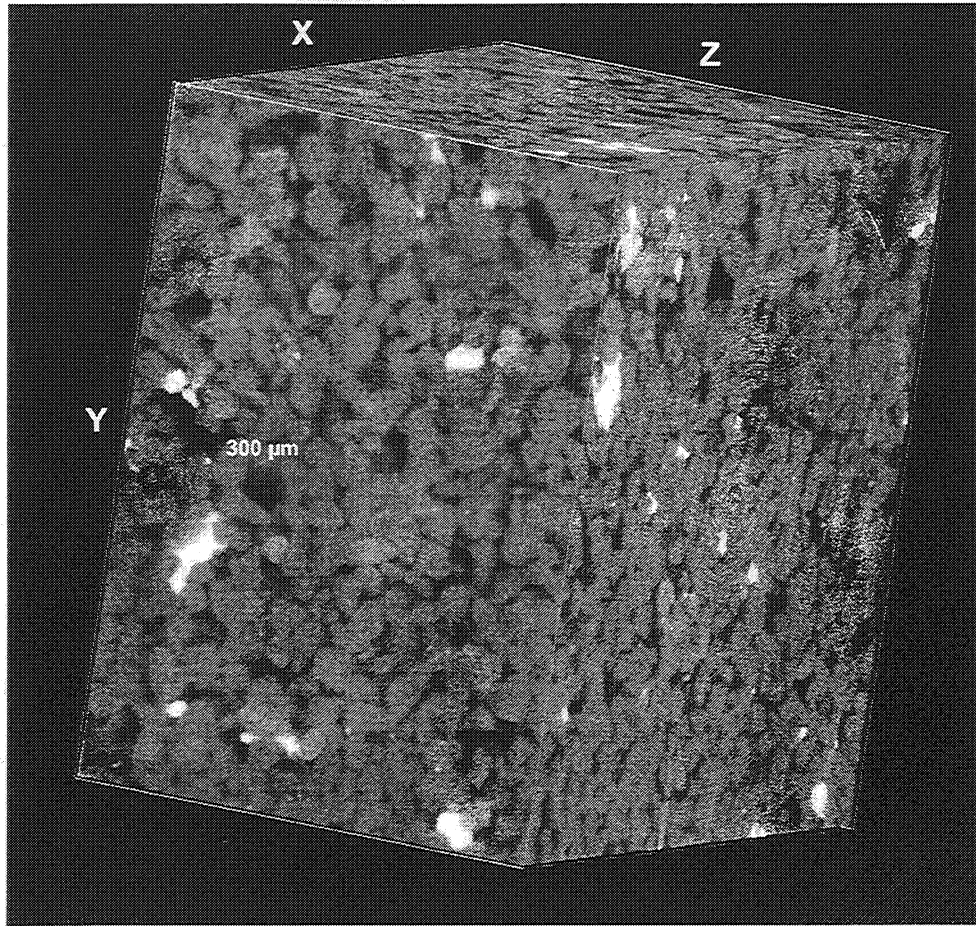


Fig. 10—3-D image of the Berea core plug with an image resolution of 10 μm ($x=4.6\text{ mm}$, $y=4.6\text{ mm}$, $z= 3.25\text{mm}$).

Since it is difficult to see through the 3-D structure, we begin by focusing on a thin slab that cuts through the x - y plane (Fig. 11). The direction of flow during fluid injection is perpendicular to the x - y plane. There are a total of 512 image slices in the z direction. The image slab that we focused on consisted of 10 image slices (slices 460-469) with a depth of 63.5 μm . During the core experiment, we first saturated the core with brine. The image in Fig. 12 was taken after the core was saturated with brine. The gray areas in Fig. 12 are the void spaces that were saturated with brine. The areas in black are rock grains. The shaded gray areas in Fig. 12 show the change in pore shape/size as we go from the surface slice (slice 469) to the bottom slice (slice 460). Next, we oilflooded the core to residual water saturation (S_{wr}). Fig. 13 shows the distribution of oil and water after the oilflood at S_{wr} . In Fig. 13, oil is in dark gray, water is in light gray, and the rock grains are in black. As shown in Fig. 13, oil invaded most of the larger pores while the residual water remained mostly in small pores and crevices. Then, we injected water into the core until no more oil was produced. Fig. 14 shows that the residual oil occupied the center of the medium to large size pores while water formed a film around the residual oil. These observations are consistent with expectations in a strongly water-wet medium.

X = 4.6 mm, Y = 4.6 mm, Z = 3.25 mm
Number of Image Slices (Z-direction) = 512

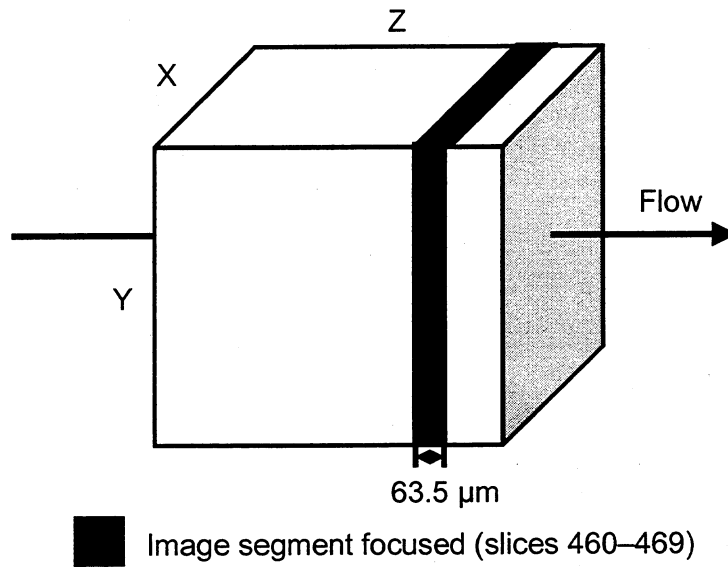


Fig. 11—Dimensions of image slab.

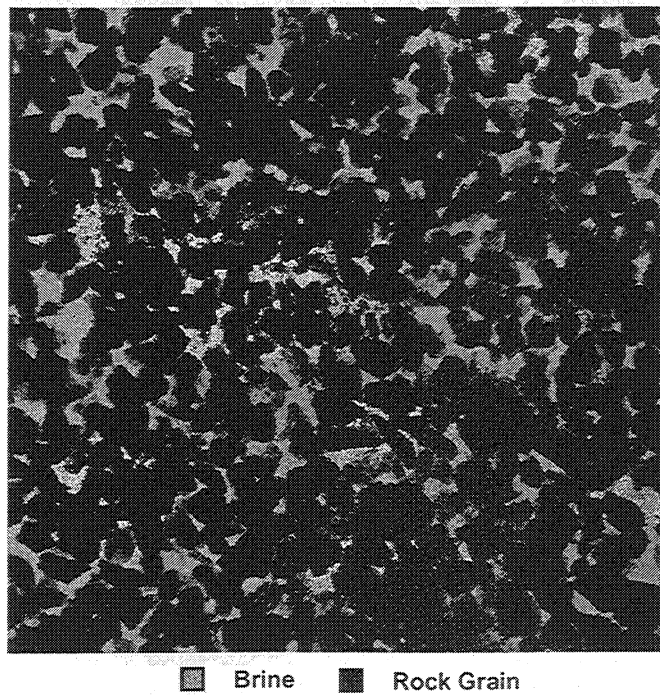


Fig. 12—*x-y* plane view of image slab (slices 460-469) at $S_w=1.0$; image resolution=10 μm.

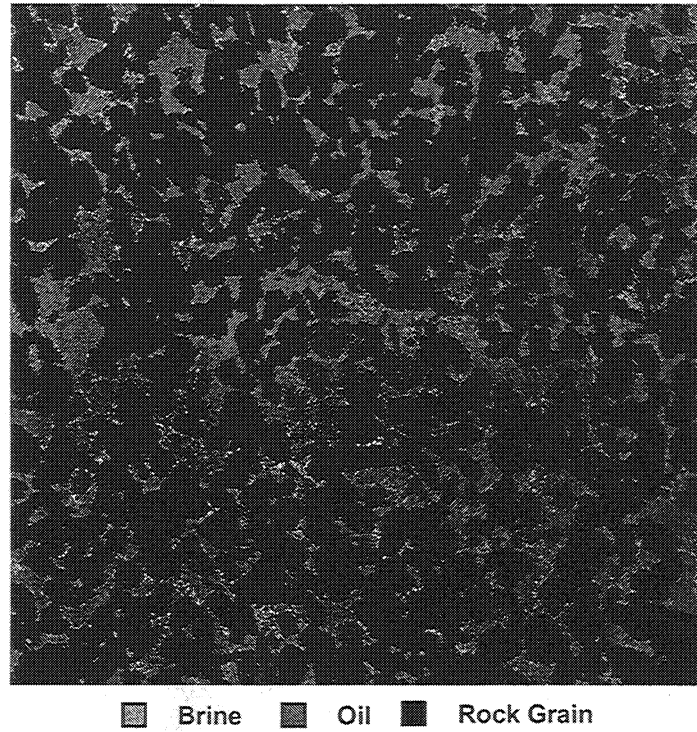


Fig. 13— x - y plane view of image slab (slices 460-469) at S_{wr} ; image resolution= $10\ \mu\text{m}$.

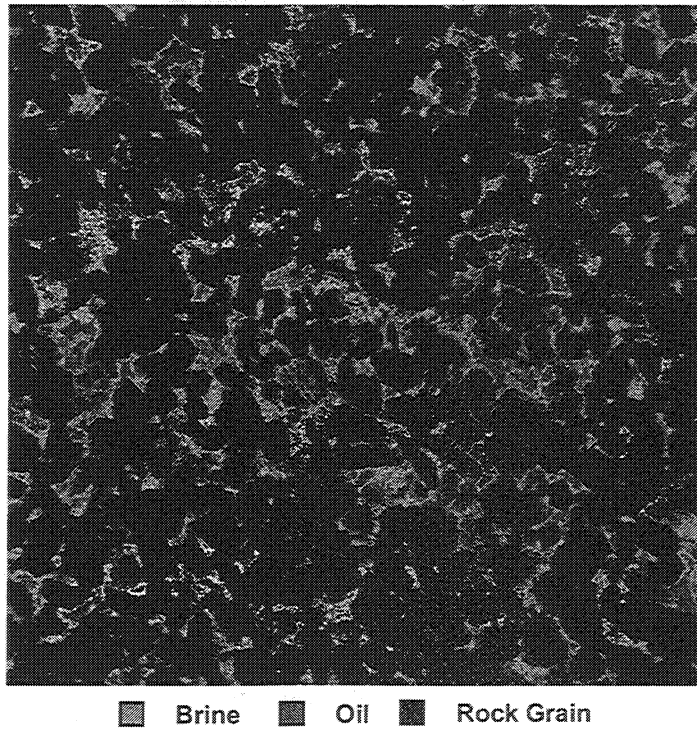


Fig. 14— x - y plane view of image slab (slices 460-469) at S_{or} ; image resolution= $10\ \mu\text{m}$.

Next, gelant was injected at residual oil saturation. Fig. 15 shows that some of the oil was displaced by the more viscous gelant during gelant injection. After gelant injection, we raised the temperature to around 60°C and shut the core in for 12 hours to allow gelation to occur. Immediately after shut-in, we injected oil to measure F_{rro} . Fig. 16 shows the distribution of oil and water after the F_{rro} measurement. Table 1 shows that the F_{rro} was 15. A comparison of Figs. 13 and 16 indicates that most of the pathways open to oil flow before gel placement remained accessible to oil after the gel treatment. This result suggests that the gel occupied only a small fraction of the pore space. Tracer results from a previous oil/water experiment in a high-permeability Berea core revealed that the gel with a F_{rro} value of 20 occupied less than 5% of the pore space. After the F_{rro} measurement, we injected brine to measure F_{rrw} . Table 1 shows that the F_{rrw} was 1,220, which was significantly higher than the F_{rro} value of 15. Fig. 17 shows that water did not have access to most of the pathways opened to oil flow after treatment. A possible explanation is that gel particles strategically positioned at the entrance of the larger pores changed the aspect ratio of the pores and rendered the oil immobile during the subsequent water injection. During water injection after gel treatment, the trapped residual oil forced the water to flow around it as a thin film or through other smaller pores. This resulted in much more constricted pathways for water after gel placement. In contrast, the oil pathways were much less constricted during oil injection after gel treatment because oil could flow through the center of the larger pores. To test this concept, detailed image analyses will be performed to quantify the size distribution of the pores that constitute the oil pathways.

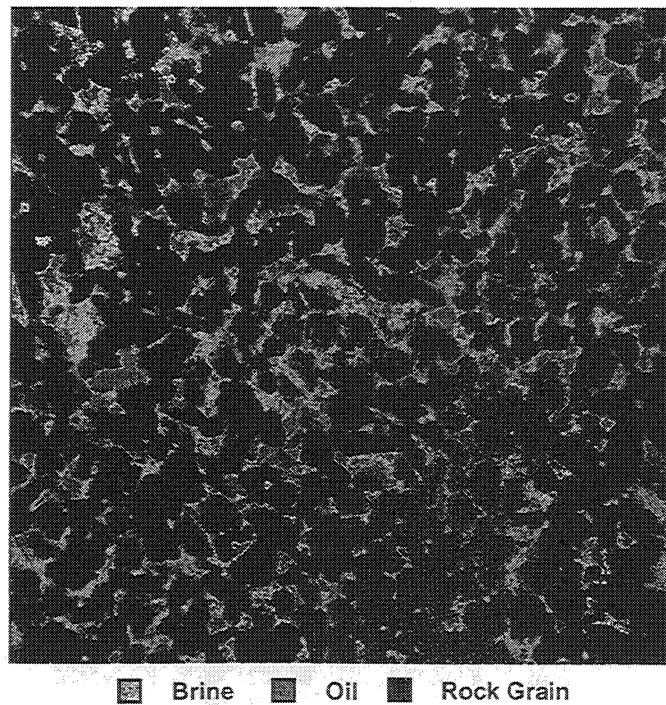


Fig. 15— x - y plane view of image slab (slices 460-469) at S_{or} after gelant injection; image resolution=10 μ m.

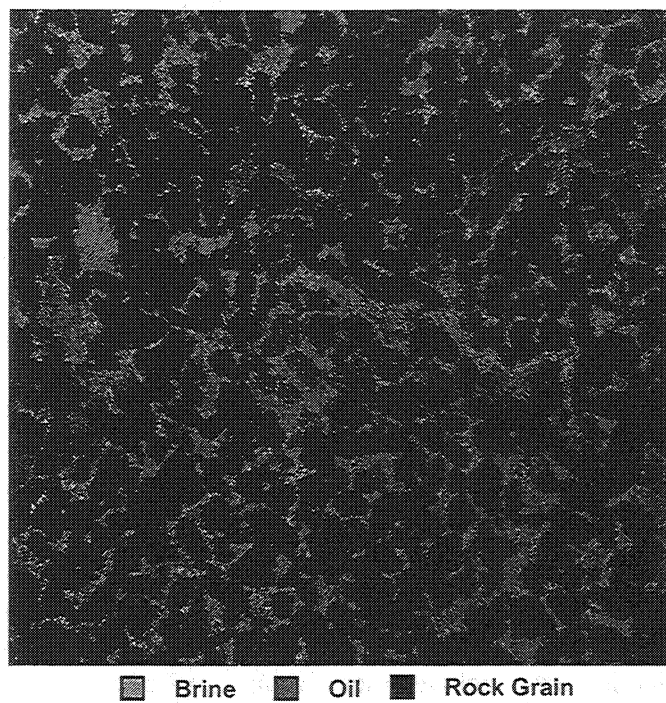


Fig. 16— x - y plane view of image slab (slices 460-469) after F_{rr0} measurement ($F_{rr0} = 15$); image resolution= $10\ \mu\text{m}$.

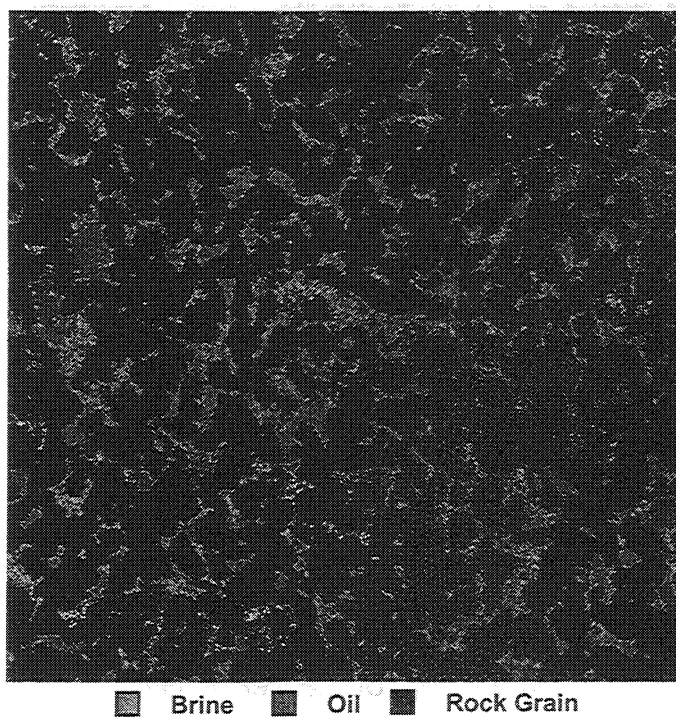


Fig. 17— x - y plane view of image slab (slices 460-469) after F_{rrw} measurement ($F_{rrw} = 1,220$); image resolution= $10\ \mu\text{m}$.

Effect of Temperature on Disproportionate Permeability Reduction. Most of our previous oil-water experiments were performed at 41°C. Since many gel treatments are performed in high-temperature reservoirs, there is a growing interest among our sponsors in understanding the effect of temperature on the disproportionate permeability reduction. To address this issue, we performed oil-water experiments at 60°C and 80°C. For each temperature, we performed two similar oil-water experiments in high-permeability Berea cores. In one experiment, oil was injected immediately after shut-in to determine the F_{rro} , while in the other, water was injected immediately after shut-in to measure F_{rrw} . The gel was our standard Cr(III)-acetate HPAM. Soltrol-130 was the oil phase. Table 2 shows F_{rrw} and F_{rro} . The ratio, F_{rrw}/F_{rro} decreased from 240 to 34 when the temperature was raised from 41°C to 60°C. However, when the temperature was raised further to 80°C, F_{rrw}/F_{rro} reversed direction and increased to 142. Thus, the effect of temperature on the disproportionate permeability is not obvious and requires further study.

Table 2. Effect of temperature on disproportionate permeability reduction.

Core: strongly water-wet Berea
Gel: 0.5% HPAM, 0.0417% Cr(III)-acetate, 1% NaCl, 0.1% CaCl₂

Temperature, °C	F_{rrw}	F_{rro}	F_{rrw}/F_{rro}
41	10,100	42	240
60	30,100	880	34
80	25,410	178	142

SUMMARY

1. During extrusion of gels through fractures, a simple relation ($u_l = 0.05 t^{0.55}$, where u_l is water leakoff rate in ft³/ft²/d or ft/d and t is time in days) described gel dehydration over a wide range of conditions. A model based on this equation was applied to estimate how far gels penetrate into two-wing fractures, as a function of injection rate and fracture width.
2. To maximize gel penetration along a given fracture, gel should be injected at the highest practical injection rate.
3. Imaging experiments are in progress using high-resolution computed microtomography (CMT) at Brookhaven National Laboratory to understand why gels reduce permeability to water more than that to oil. The method provides outstanding resolution of rock, water, and oil on a micrometer scale. In water-wet Berea sandstone, the water film around trapped residual oil drops was clearly visible. In our first set of experiments, CMT results indicated that gels increased the residual oil saturation in larger pores during water injection, thus decreasing permeability to water much more than that to oil.
4. With a Cr(III)-acetate-HPAM gel in water-wet Berea sandstone, the disproportionate permeability reduction was substantial at temperatures of 41°C, 60°C, and 80°C. Water permeability was reduced 34 to 240 times more than that to oil. Additional work is required to understand details of the effects of temperature on the disproportionate permeability reduction.

REFERENCES

1. Seright, R.S.: "Using Chemicals to Optimize Conformance Control in Fractured Reservoirs," Annual Technical Progress Report (U.S. DOE Report DOE/BC/15110-2), U.S. DOE Contract DE-AC26-98BC15110, (Sept. 1999) 3-52.
2. Howard, G.C. and Fast, C.R.: *Hydraulic Fracturing*, SPE Monograph Series, 2, Society of Petroleum Engineers, Dallas (1970) 33.
3. Seright, R.S.: "Gel Propagation Through Fractures," paper SPE 59316 presented at the 2000 SPE/DOE Improved Oil Recovery Symposium, Tulsa, April 3-5.
4. Seright, R.S.: "Mechanism for Gel Propagation Through Fractures," paper SPE 55628 presented at the 1999 Rocky Mountain Regional Meeting, Gillette, May 15-18.
5. Seright, R.S.: "Improved Techniques for Fluid Diversion In Oil Recovery," final report, DOE/BC/14880-15, U.S. DOE (Jan. 1996) 97-108.
6. Coles, M.E., Hazlett, R.D., Muegge, E.L., Jones, K.W., Andrews, B., Dowd, B., Siddons, P., Peskin, A., Spanne, P., and Soll, W.E.: "Developments in Synchrotron X-Ray Microtomography with Applications to Flow in Porous Media," paper SPE 36531 presented at the 1998 Annual Technical Conference and Exhibition, Denver, Oct. 6-9.

